

Carbomer Hydrogel Composed of Cu₂O and Hematoporphyrin Monomethyl Ether Promotes the Healing of Infected Wounds

Dongyu Wang, Jiale Jin, Chengran Zhang, Chengxin Ruan, Yifang qin, Dongdong Li, Ming Guan,* and Pengfei Lei*



Cite This: *ACS Omega* 2024, 9, 4974–4985



Read Online

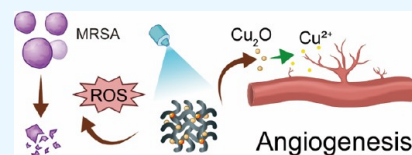
ACCESS |

Metrics & More

Article Recommendations

Supporting Information

ABSTRACT: Infectious wounds pose a significant challenge in the field of wound healing primarily due to persistent inflammation and the emergence of antibiotic-resistant bacteria. To combat these issues, the development of an effective wound dressing that can prevent infection and promote healing is of the utmost importance. Photodynamic therapy (PDT) has emerged as a promising noninvasive treatment strategy for tackling antibiotic-resistant bacteria. A biodegradable photosensitizer called hematoporphyrin monomethyl ether (HMME) has shown potential in generating reactive oxygen species (ROS) upon laser activation to combat bacteria. However, the insolubility of HMME limits its antibacterial efficacy and its ability to facilitate skin healing. To overcome these limitations, we have synthesized a compound hydrogel by combining carbomer, HMME, and Cu₂O nanoparticles. This compound hydrogel exhibits enhanced antimicrobial ability and excellent biocompatibility and promotes angiogenesis, which is crucial for the healing of skin defects. By integrating the benefits of HMME, Cu₂O nanoparticles, and the gel-forming properties of carbomer, this compound hydrogel shows great potential as an effective wound dressing material. In summary, the compound hydrogel developed in this study offers a promising solution for infectious wounds by addressing the challenges of infection prevention and promoting skin healing. This innovative approach utilizing PDT and the unique properties of the compound hydrogel could significantly improve the outcomes of wound healing in clinical settings.



1. INTRODUCTION

Delay healing of skin defects would induce diverse negative effects, such as infection. Antibiotic is the main strategy of antibacteria in curing infectious skin defect. However, due to the overdose or abuse of antibiotics, antibiotic resistance has become a serious problem.¹ The use of antibiotics alone makes it difficult to achieve effective antibacterial. Photodynamic therapy (PDT) is a newly developed strategy for disease diagnosis and treatment using photodynamic effects.² When photosensitizers were triggered and activated by laser in a given wavelength, the local reactive oxygen species (ROS) would increase and destroy the cell structure such as cell membrane, protein and even nucleic acids.³ This method has a different mechanism than traditional antibiotics, which enables antibiotic resistance could be controlled in a new way.⁴ It is well-known that PDT processes advantages such as fewer side effects and localized treatment.⁵ However, the solubility of photosensitizers is poor, and it is difficult to achieve effective drug concentrations.⁶

Even if diverse photosensitizers have already been applied in clinical treatment, there still exists some concern for biocompatibility and other problems. Meanwhile, it could be concluded that a suitable strategy would help hydrogel overcoming these problems.⁷ For instance, photosensitizers like silica are nondegradable and could cause harm.⁸ To forbid this side effort, we chose hematoporphyrin monomethyl ether (HMME) as the major ingredient for the compound wound

dressing material. HMME is safe enough that it has already been applied in various patients by the PDT strategy.^{9,10} Meanwhile, HMME can combine with CBMG by electrostatic adsorption. In addition, metal ions are other elements that have antibacterial activities, so as metallic oxide.¹¹ Cu₂O nanoparticles are also a kind of photosensitizer that would produce ROS to kill bacteria. Apart from this concern, the copper ions Cu₂O nanoparticles releasing would contribute to antibacterial and angiogenesis.¹² Carbomer 940 is an ideal hydrogel that could be degraded and cause no side effects.¹³ In addition, Cu₂O nanoparticles triggered by the laser would produce photogenerated electron–hole pairs that would contribute to antibacterial, which is called the hole effect.¹⁴ These character makes it a brilliant choice serving as a carrier of drugs and a basic wound dressing material. In brief, a compound hydrogel system for skin curing was completed.

In this study, a combined CBMG-Cu₂O-HMME hydrogel was synthesized with photostability and stability. The ingredients such as HMME and Cu₂O can contribute to antibacterials in the case of skin effect infection. The laser

Received: November 15, 2023

Revised: December 24, 2023

Accepted: December 28, 2023

Published: January 16, 2024



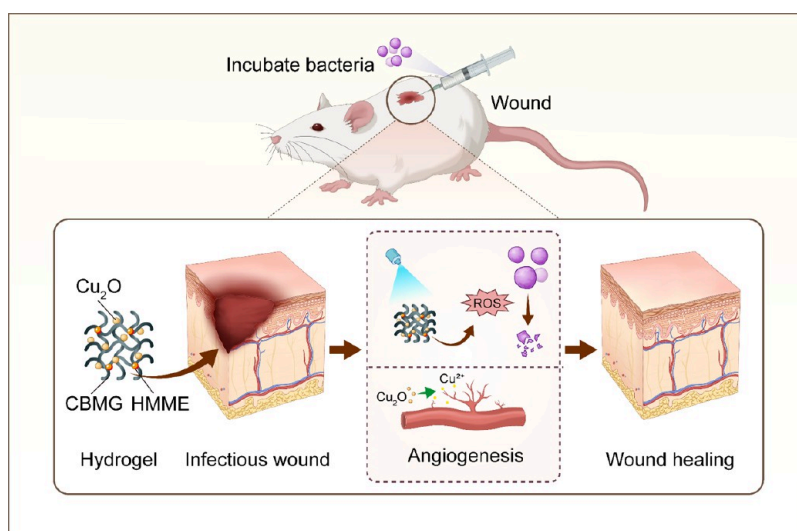


Figure 1. Graphical abstract. Schematic illustration of antibiosis and angiogenesis by the CBMG- Cu_2O -HMME hydrogel for infected wound healing. CBMG: carbomer. HMME: hematoporphyrin monomethyl ether. Cu_2O : Cu_2O nanoparticles.

lighting of HMME and Cu_2O enhances this capacity. In addition, copper ions Cu_2O released could also prompt formation of vessels, which would do well for skin defect curing. As expected, the compound hydrogel we developed exerts brilliant antibacterial and angiogenesis. In a word, the ideal performance of combined hydrogel indicates that it has the potential to be applied in wound dress. The function of this CBMG hydrogel is demonstrated in Figure 1.

2. MATERIALS AND METHODS

2.1. Reagent. Triethanolamine (in liquid, > 99.5%) and Carbomer 940 (in powder, 99.0%) were taken from Macklin Reagent Co., Ltd. (Shanghai, China). Cu_2O nanoparticles were purchased from Beijing TianDun Advanced Materials Technology Co., Ltd. (Beijing, China). Hematoporphyrin monomethyl ether (HMME) was purchased from MedChemexpress (America). Methicillin-resistant *Staphylococcus aureus* (MRSA, ATCC43300) and extended-spectrum β -lactamase-producing *Escherichia coli* (ESBL *E. coli*, ATCC35218) were given by the Lab of Microbiology of the author's college. Human umbilical vein endothelial cells (HUVEC) were provided by our lab. Basement membrane matrix was purchased from MedChemexpress (America). DAPI and TRITC were purchased from Solarbio (Solarbio, China). CCK 8 kits were purchased from Beyotime Biotechnology (China).

2.2. Fabrication of CBMG- Cu_2O -HMME. CBMG hydrogel was synthesized according to the method of ref 15. Two grams of carbomer was dissolved in 100 mL of double-distilled H_2O (dd H_2O) and stirred in a 60 °C water bath for 30 min. Then, the pH was adjusted to 6.5–7.5 with 0.25 mL triethanolamine. Finally, nanometer cuprous oxide powder and HMME in powder form were added to CBMG. According to the group, the concentration of Cu_2O was tested to determine the ideal content, 0, 0.5, 5, 10, 50, and 100 mg/L. According to the research on HMME,¹⁶ the concentration of HMME was chosen as 10 $\mu\text{g}/\text{mL}$. The HMME was mixed with CBMG powder as the concentration above, and then the mixture was dissolved in dd H_2O . Next, the mixture was subjected to magnetic stirring for 30 min and then stored at 37 °C environments for about 24 h. The prepared CBMG, CBMG- Cu_2O , CBMG-HMME, and CBMG- Cu_2O -HMME

were rinsed 3 times with dd H_2O and stored in a refrigerator at 4 °C. The CBMG hydrogels every experiment used were synthesized in 24 h.

2.3. Characterization of CBMG with HMME and Cu_2O .

The micromorphology of CBMG, CBMG- Cu_2O , CBMG-HMME, and CBMG- Cu_2O -HMME was observed using scanning electron microscopy (Quanta-200, FEI, Netherlands). Simply put, this series of hydrogels was frozen overnight at the temperature of -80 °C and then lyophilized for 48 h, followed by vacuum gold spraying for 10 min and finally SEM observation. CBMG- Cu_2O -HMME was detected by NMR (Avance-400, Germany). Rheology is used to measure viscosity (rotational rheometer model: MARS 60, HAAKE, Germany). Test conditions are as follows: frequency $f = 1$ Hz, shape variable $\gamma = 1\%$, temperature from 10 to 45 °C, 5 °C per minute. G' is the elastic modulus (energy storage) and G'' is the viscous modulus (loss). The composition of the hydrogel is detected by infrared (Fourier infrared spectrometer model: Nicolet iS50).

2.4. Evaluation of Cytocompatibility. Cuprous oxide nanoparticles of different concentrations were cocultured with human umbilical vein endothelial cells (HUs), and the following experiments were carried out at their respective time points.

Cytoskeleton staining was done after incubation for 24 h. HUs were fixed with 4% PFA for 2 h. The cell membrane was penetrated by 0.1% TritonX-100 (Thermo Scientific, America) for 10 min, and then TRITC (Sigma, China) was added to stain for 60 min and cleaned with PBS for 3 times, 5 min at a time. Finally, the DAPI solution (Sigma, China) was applied and incubated at room temperature for 10 min without light. Then, it was washed with PBS 3 times for 5 min. Finally, the images were observed and photographed under a fluorescence microscope (Olympus FV3000, Tokyo, Japan).

Live/dead cell staining was done after 1 day of culture. The HUs were pretreated with AM and PI. After buffer removal, a staining solution (Beyotime Biotechnology, China) was added to recognize living and dead human umbilical vein endothelial cells. After culturing for 10 min, PBS was used to wash 3 times for 5 min every time. Finally, HUs were observed and

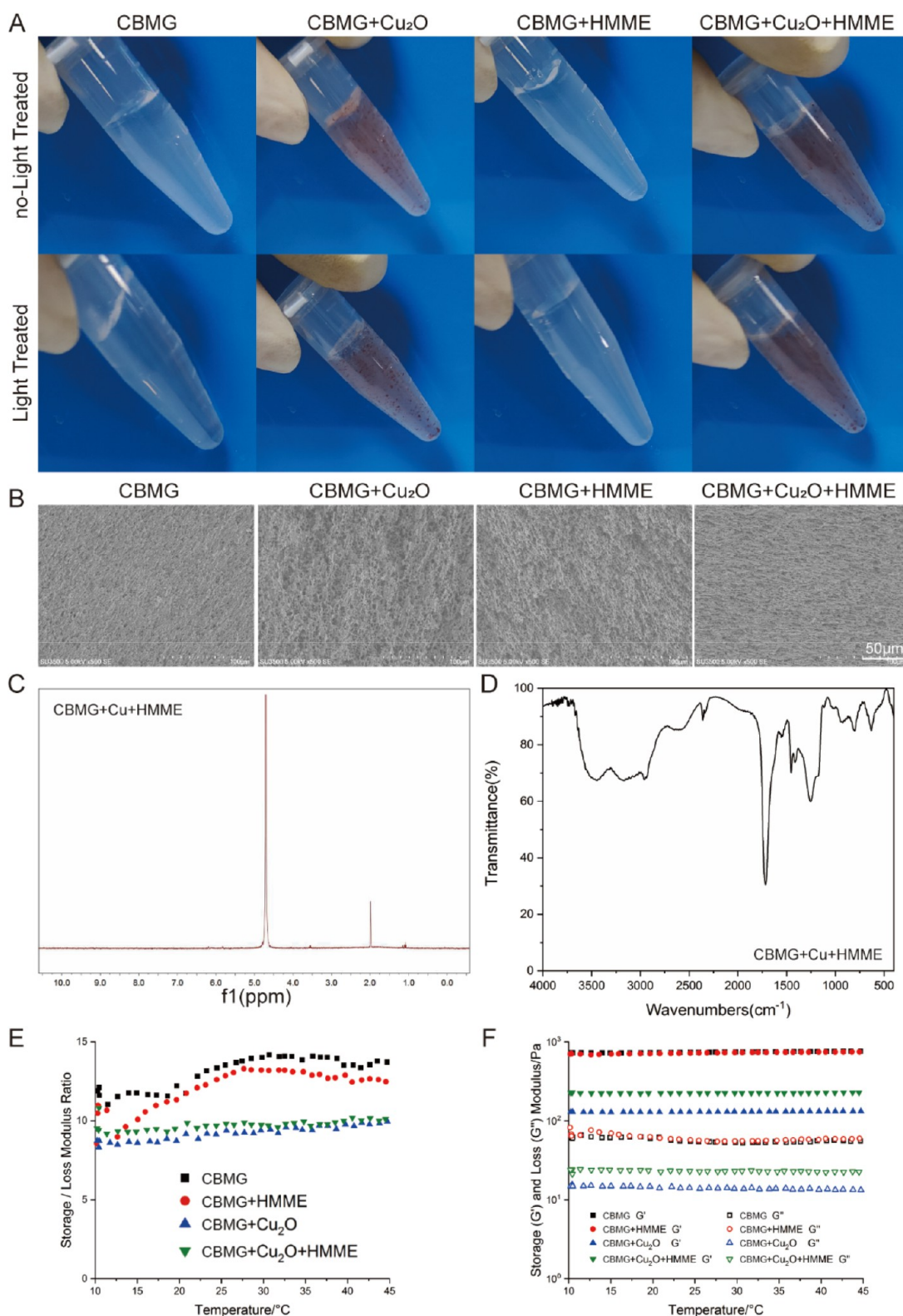


Figure 2. (A) Representative images of the CBMG hydrogel packed with various elements. (B) Representative SEM results of CBMG loaded with various elements. (C) Nuclear magnetic resonance hydrogen spectroscopy of the CBMG-Cu₂O-HMME hydrogel. (D) Fourier infrared spectroscopy of the CBMG-Cu₂O-HMME hydrogel. (E, F) Rotary rheometer was used to measure the hydrogels' elastic modulus (G') and storage modulus (G''), as well as the storage/loss modulus ratio.

photographed by a fluorescence microscope (Olympus FV3000, Tokyo, Japan).

CCK8 1×10^4 HUs were treated with cuprous oxide nanoparticles of different concentrations, and 10% CCK8

reagent was added after 12 and 24 h of treatment. After incubation for 2 h, the supernatant was absorbed to detect the absorbance at 450 nm by a microplate reader (Thermo Scientific, America). The ratio of each group to the control

group was quantitatively analyzed using the CBMG group as a reference, which has no Cu₂O nanoparticles.

2.5. Evaluation of Angiogenesis. HU cell migration was evaluated by a Transwell assay (3422, Corning, USA). HU cells (2×10^4) were inoculated into the upper cavity. A complete medium containing cuprous oxide nanoparticles of various concentrations with a volume of 500 μ L was added to the lower cavity. Every group was cultured at 37 °C with 5% CO₂ for 12 h. The cells were then immobilized, stained, microscopically imaged (Olympus IX 70, Tokyo, Japan), and counted using ImageJ software.

Angiogenesis matrix glue was stored at -20 °C. It should be thawed at 4 °C overnight. After it became a liquid station, each hole of the 48-well plate was coated with 100 μ L of matrix glue. Then, the plates were placed in a 37 °C environment for 1 h. After matrix glue was solidified, 1×10^4 HU cells were added, and cuprous oxide nanoparticles with corresponding concentration were added to each hole. After coculturing at 37 °C for 12 h, the results were observed and photographed under an inverted microscope. The results were analyzed with ImageJ.

Cell migration: 1×10^5 HU cells were added into each hole of the 6-well plate and shaken well. When overgrown, a 1000 μ L gun tip was used to make a straight line in the hole, and then cuprous oxide nanoparticles with the corresponding concentration were added to each hole, which was cocultured at 37 °C for 12 and 48 h, observed under an inverted microscope, and photographed. The results were analyzed with ImageJ. The area of scratch was calculated and compared with the control group for quantitative analysis.

2.6. Evaluation of Antibacterial Activity In Vitro. The in vitro antibacterial activity of MRSA (G+) and ESBL *Escherichia coli* (G-) was evaluated by the laser triggering method. Trypsin bean soup (TSB) medium was used to culture bacterial overnight. Then, bacteria was harvested at the accelerated growth phase. After centrifugation, the concentration of every bacterium was altered to 1×10^8 CFUs/mL and redispersed with fresh PBS. CBMG, CBMG-Cu₂O, CBMG-HMME, and CBMG-Cu₂O-HMME were added into 1 mL of suspension, which contains MRSA or ESBL *E. coli* (about 1×10^6 CFUs/mL), respectively. After that, they were lighted with laser (600 nm, 175 mW/cm²) for about 10 min¹⁷. Each group was compared with the group that was not exposed to laser light. The antibacterial activity was evaluated by using planking and scanning electron microscopy. The count of viable bacteria after different treatments was carried out by using the planking method. To put it simply, 100 mL of bacterial suspension is continuously diluted, dripped on the blood AGAR plates, and then cultured at the temperature of 37 °C overnight. Colonies on each plate were counted. The performance quantitative analysis method is used to compare the number of colonies in each group and the ratio of the CBMG group. Morphological changes in *Escherichia coli* MRSA and ESBL were observed by scanning electron microscopy. The resulting samples with bacteria were washed two times by PBS, then fixed with 4% paraformaldehyde at 4 °C for 6 h, and then dehydrated in an ethanol–water mixture (30, 50, 70, 85, 90, 95, and 100%) for 15 min. The bacteria were then cryo-dehydrated and sprayed with gold before being observed under scanning electron microscopy (Regulus8100, Hitachi, Japan).

2.7. Evaluation of Skin Healing In Vitro. The antibacterial capacity of the composite hydrogel was estimated

by the MRSA infection wound model in SD rats. Eighty SD female rats (8 weeks old, 250 g) were fed in a sterile environment. 2% pentobarbital sodium was used to anesthetize SD rats by injection of intraperitoneally. The hair on the back is shaved and disinfected, and a full skin wound of 8 mm in diameter is created with a surgical blade. Before that, the MRSA suspension cultured overnight was washed with fresh PBS and collected. Finally, MRSA suspension (10^7 CFUs/cm²) was then applied to the wound.

After 2 days, they were randomly divided into four groups (3 animals/group) according to the treatment method, including CBMG, CBMG-Cu₂O, CBMG-HMME, and CBMG-Cu₂O-HMME. The wound was recorded after the operation, and this time was set at day 0. Wound area was calculated by ImageJ (V1.53, NIH, Bethesda, MD, USA) at 3 and 14 days after surgery to assess wound healing. Obvious time points were chosen according to the previous research.¹⁵ The wound area of the control group serves as a standard for quantitative analysis of the related healing area to assess the efforts of every group.

Four groups of rats were treated with hydrogel after 10 min of laser irradiation (175 mW/cm²) on day 2024/01/15. On days 7 and 14, rats in each group were randomly selected for histological examination. The rats were killed with an overdose of anesthesia, and tissue around the skin wound was collected and cut in half. The tissues were fixed with 4% glutaraldehyde and embedded in paraffin for histological studies, which contains HE staining, Sirius red staining, and Masson staining. After 14 days of operation, all rats were killed by excessive anesthesia, and wound tissue was collected and stained with HE, Sirius red, and Masson. The neovascularization of the wound skin was evaluated at 3 and 14 days after operation, and the proportion of neovascularization was quantitatively analyzed by immunofluorescence double staining with CD31 and α -SAM antibodies, respectively.

2.8. Statistical Analysis. All quantitative data were shown as mean \pm standard deviation (SD). As for the analysis method, one-way analysis of variance (ANOVA) was applied for data, as appropriate. A *P* value of 0.05 (*, *P* < 0.05) was considered statistically significant.

3. RESULTS AND DISCUSSION

In this research, we combined a carbomer hydrogel with Cu₂O and HMME to get a CBMG-Cu₂O-HMME hydrogel through electrostatic interaction. Compared with Cu₂O or HMME alone, the CBMG-Cu₂O-HMME hydrogel exhibits enhanced photoactivated antibacterial activity. The results of each experiment were listed and discussed as follows.

3.1. Photophysical Characterization of CBMG Hydrogels. CBMG is semitransparent. It is seen that the laser treatment does not influence the appearance of CBMG and the other hydrogels (Figure 2 A). A porous structure was observed in every group detected by scanning electron microscopy (SEM), which indicated that elements such as HMME and Cu₂O will not prompt or inhibit the gel-forming (Figure 2 B). Nuclear magnetic resonance (NMR) and infrared spectroscopy analysis confirmed that the final hydrogel consisted of CBMG, Cu₂O, and HMME (Figure 2C,D). The rheological testing was used to determine the gel formation (Figure 2E,F). Double bond signal peaks in carbomer were detected at 5.8 and 6.2 ppm in NMR, indicating the introduction of carbomer into the hydrogel. At 1560 cm⁻¹ in the IR, carbomer was detected in the double bond in the signal peak, which suggests the

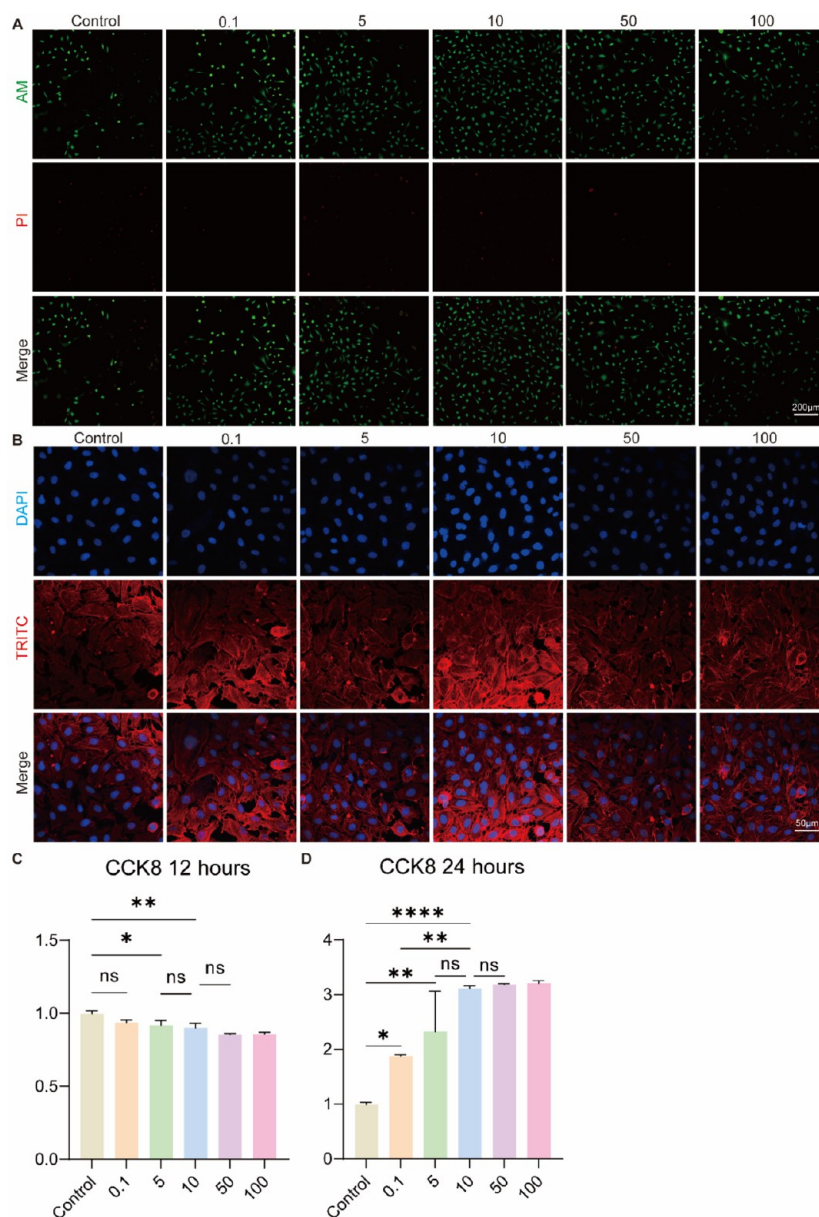


Figure 3. (A) Live and dead staining of HUs after 24 h culturing with different Cu₂O nanoparticle concentrations. (B) DAPI and TRITC staining of HUs after 24 h culturing with different Cu₂O nanoparticle concentrations. (C) CCK8 test of HUs after 12 h culturing with different Cu₂O nanoparticle concentrations ($n = 3$). (D) CCK8 test of HUs after 24 h culturing with different Cu₂O nanoparticle concentrations ($n = 3$). * ($P < 0.05$), ** ($p < 0.01$), *** ($p < 0.001$), and **** ($p < 0.0001$).

introduction of carbomer in the hydrogel. The Cu₂O nanoparticles are distributed evenly in CBMG (Figure S1). These tests show that a serious CBMG hydrogel was formed with the content of HMME and Cu₂O. The HMME with positive charges could combined with CBMG by negative charges, which could enhance the solubility of HMME. Meanwhile, this combination could also contribute to the CBMG hydrogel-forming. In a word, this system is an ideal combination hydrogel for wound dressing materials.

In this section, various tests were conducted to characterize the properties of the CBMG hydrogels. We found that the hydrogel remained transparent after laser treatment and had a porous structure, as observed under a scanning electron microscope. Nuclear magnetic resonance (NMR) and infrared spectroscopy analysis confirmed the presence of CBMG, Cu₂O, and HMME in the hydrogel. Rheological testing

demonstrated the formation of CBMG hydrogels with HMME and Cu₂O. The combination of HMME and CBMG enhanced the solubility and gel-forming properties, making it an ideal hydrogel for wound dressing materials.

3.2. Biocompatibility of CBMG Hydrogels. To determine the proper content of Cu₂O nanoparticles that have less cell toxicity and a better prompt of cell proliferation,¹⁸ a cell biocompatible experiment was carried out. According to live and dead staining of HUs treated with different concentrations of Cu₂O nanoparticles, 10 μg/mL was the best choice for HUs (Figure 3A). Cell skeletons stained by TRITC and DAPI can draw the same conclusion (Figure 3B). A CCK 8 test was employed to compare the cell counts, another way to tell the influence on HUs (Figure 3C,D). It is shown that Cu₂O nanoparticles have a bad influence after coculturing for 12 h. Things are different after 24 h. The

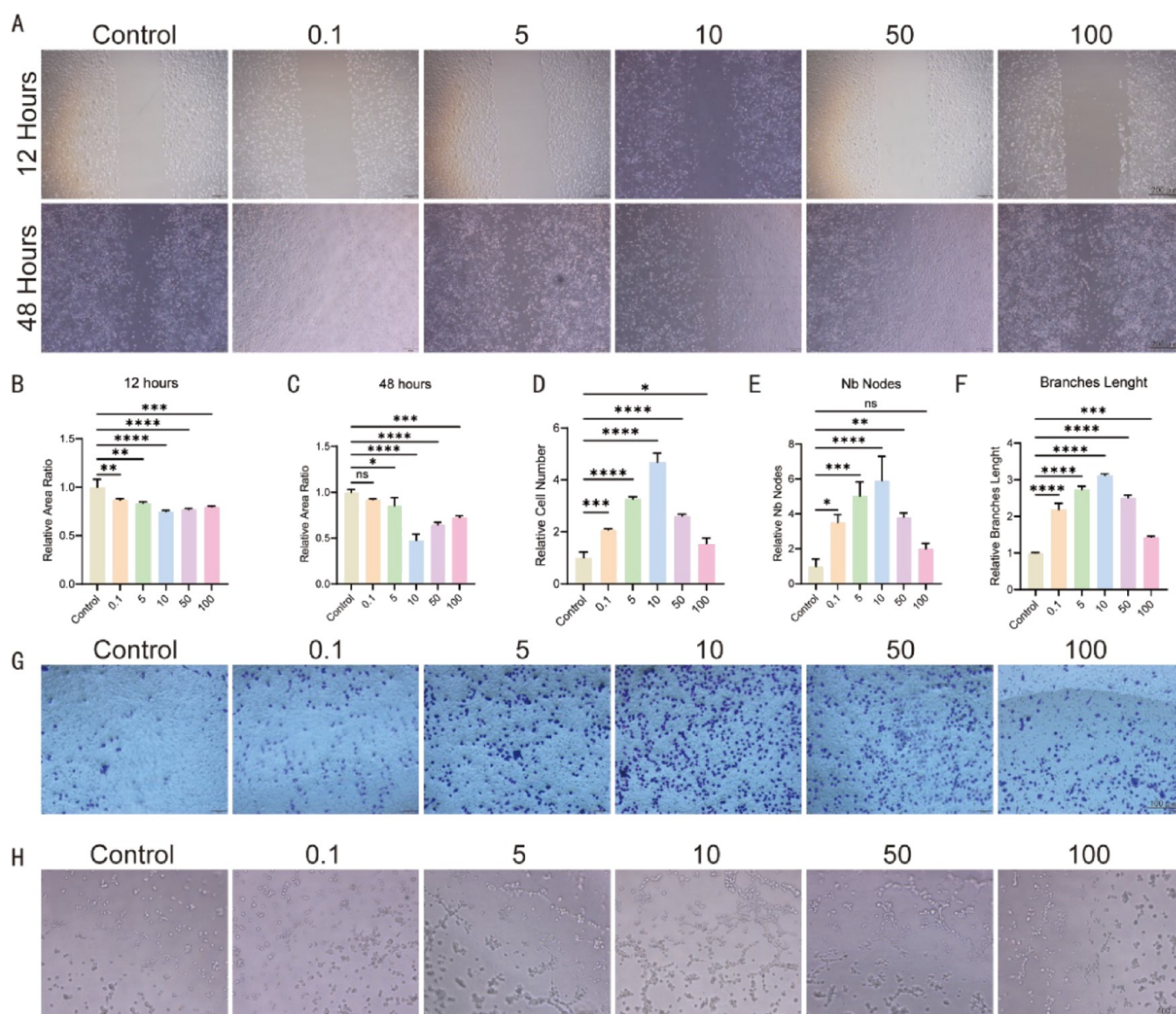


Figure 4. (A) Cell migration of HUVECs after 12 and 24 h culturing with different Cu_2O nanoparticle concentrations. (B) Quantitative analysis of cell migration after 12 h culturing with different Cu_2O nanoparticle concentrations ($n = 3$). (C) Quantitative analysis of cell migration after 24 h culturing with different Cu_2O nanoparticle concentrations ($n = 3$). (D) Quantitative analysis of transwell results ($n = 3$). (E) Quantitative analysis of the number of nodes after HUVECs culturing with different Cu_2O nanoparticle concentrations ($n = 3$). (F) Quantitative analysis of the branch length after HUVECs culturing with different Cu_2O nanoparticle concentrations ($n = 3$). (G) Transwell results after HUVECs culturing with different Cu_2O nanoparticle concentrations. (H) Angiogenesis images after HUVECs culturing with different Cu_2O nanoparticle concentrations. * ($P < 0.05$), ** ($p < 0.01$), *** ($p < 0.001$), and **** ($p < 0.0001$).

number of HUVECs was positively correlated with the concentration of Cu_2O . These findings demonstrate the correlation of HUVECs biocompatibility and Cu_2O concentration and tell the proper content that prompts HUVECs growth.

To determine the optimal concentration of Cu_2O nanoparticles that have less cell toxicity and promote cell proliferation, a biocompatibility experiment was conducted. We found that a concentration of $10 \mu\text{g/mL}$ Cu_2O nanoparticles was the best choice for human umbilical vein endothelial cells (HUVECs). Cell staining and count tests supported this conclusion, showing a positive correlation between the HUVEC biocompatibility and Cu_2O concentration.

Compared with carrying Cu^{2+} ions, Cu_2O nanoparticles could provide a long-term copper ions release that conducts a

sustaining antibacterial ability.¹⁹ Owing to the fact that skin defect should be controlled at the very beginning, this research would not explore the time of antibiotic capacity. Meanwhile, the oxidation of Cu_2O can protect HMME from inactivation and loss of antibacterial activity. In addition, the different antibiotic mechanisms of HMME and Cu_2O might result in the enhancement of the antibacterial ability. To summarize, CBMG, Cu_2O , and HMME could form a hydrogel and show the characters as we designed.

3.3. Angiogenesis Ability In Vitro. Vascularization contributes to skin healing. Copper is acknowledged to contribute to angiogenesis.²⁰ To simulate skin healing in vitro, cell migration and angiogenesis were designed, which would clarify the influence of different Cu_2O content (Figure 4A). The results show that $10 \mu\text{g/mL}$ Cu_2O nanoparticles can

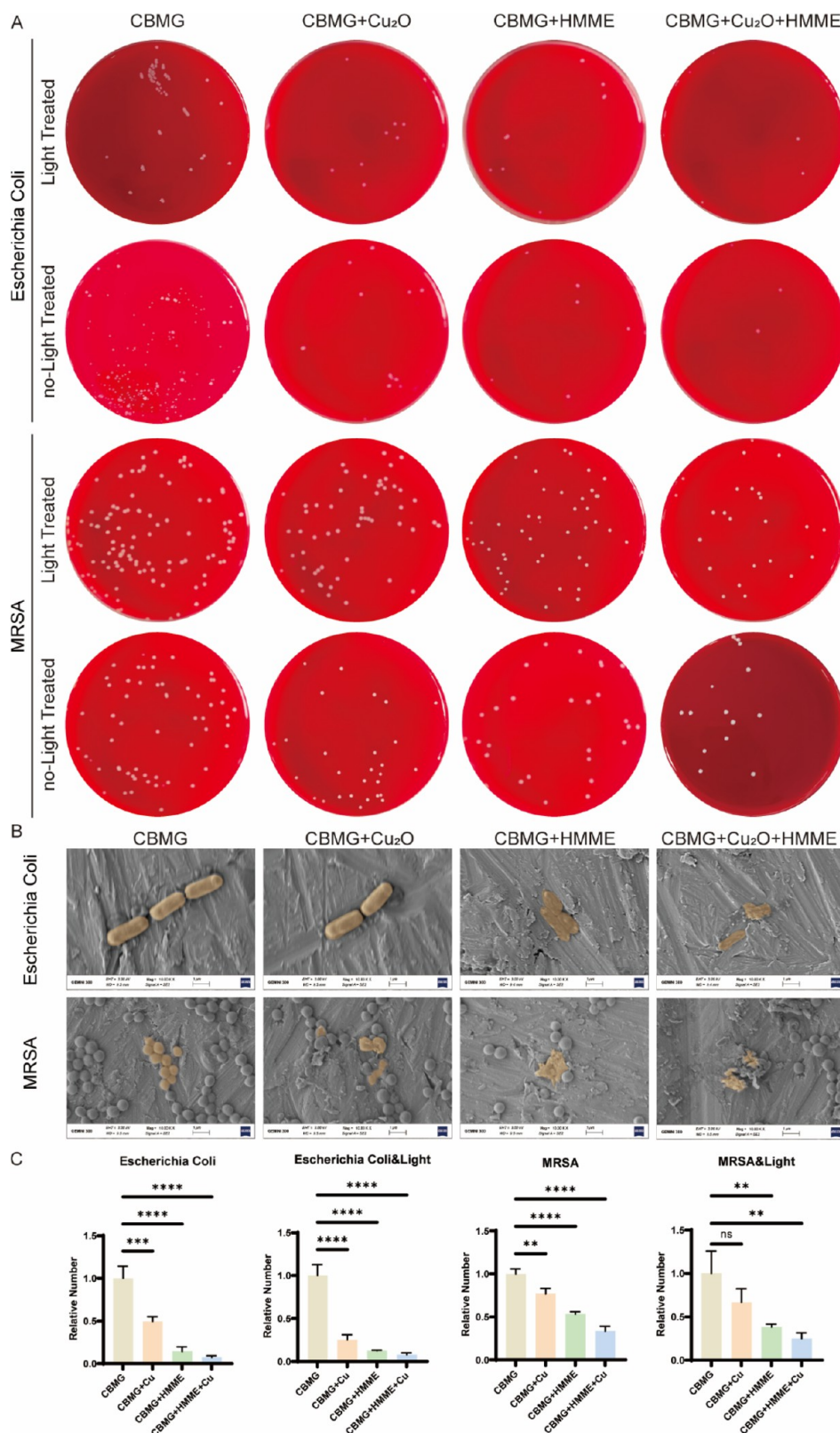


Figure 5. (A) MRSA CFUs on plates after treatment with various hydrogels with laser irradiation or without any treatment using the spread plate method. (B) Representative SEM images of MRSA after suffering various treatments. (C) Quantitative analysis of *Escherichia coli* and MRSA treated with different hydrogels with or without laser lighting ($n = 3$). * ($P < 0.05$), ** ($p < 0.01$), *** ($p < 0.001$), and **** ($p < 0.0001$).

prompt cell migration better after treating 12 h (Figure 4B). The advantage was greater after 48 h (Figure 4C). The transwell experiment is another aspect that can exhibit the attraction of cell migration (Figure 4G). Consequence also

supports 10 $\mu\text{g/mL}$ Cu₂O nanoparticles as an ideal choice (Figure 4D). Besides cell migration, angiogenesis is also an important property (Figure 4H). Quantitative analysis indicates that 10 $\mu\text{g/mL}$ is the best concentration (Figure

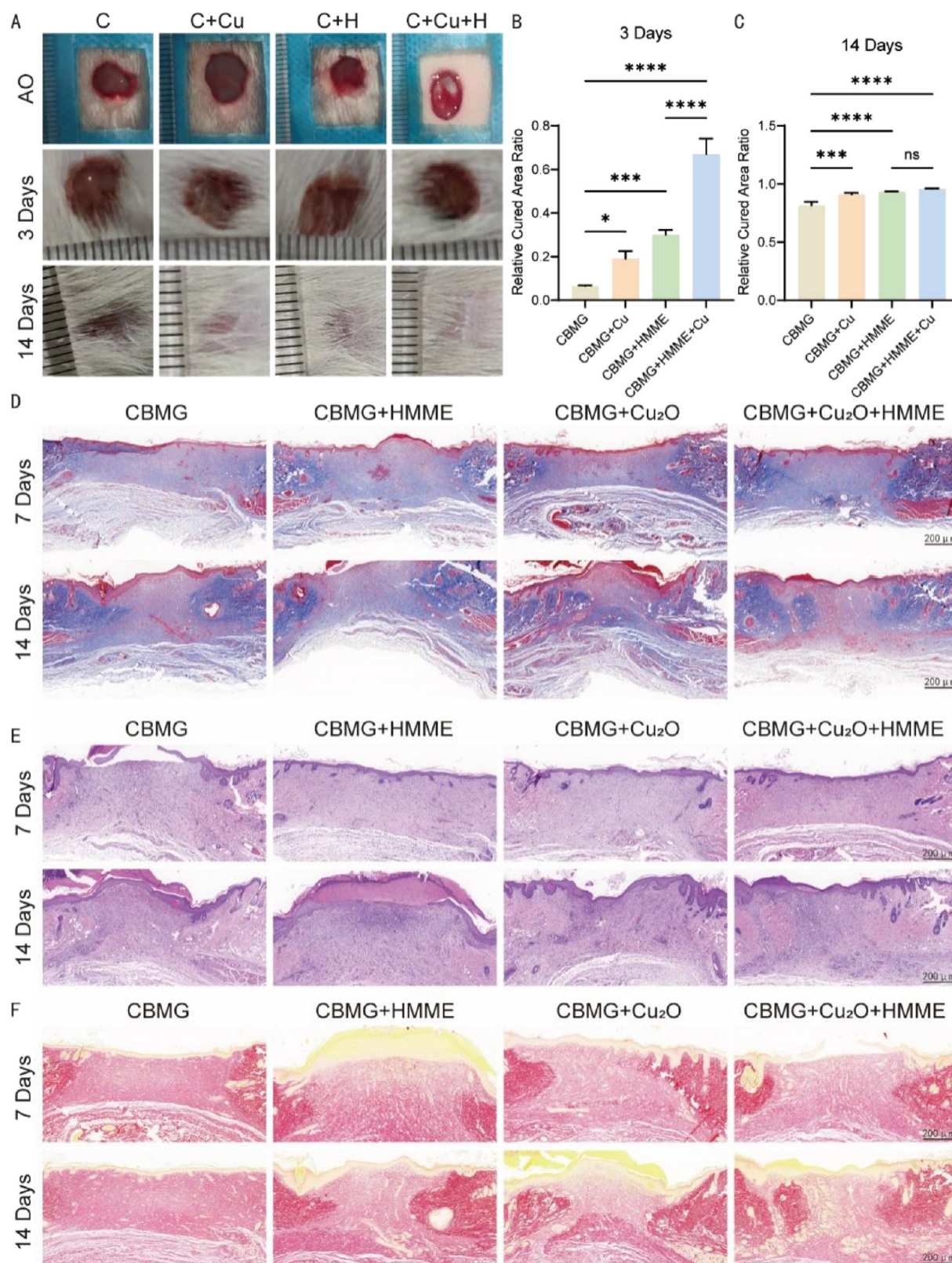


Figure 6. (A) Representative wound area on days 0, 3, and 14. (B) Relative wound healing rate 3 days after operation ($n = 3$). (C) Relative wound healing rate 14 days after the operation ($n = 3$). (D) Representative Masson staining observed in wound tissues. (E) Representative HE staining observed in wound tissues. (F) Representative Sirius red staining in wound tissues. * ($P < 0.05$), ** ($p < 0.01$), *** ($p < 0.001$), and **** ($p < 0.0001$).

4E,F). In brief, both cell biocompatible experiments and angiogenesis-related tests support 10 μ g/mL Cu₂O nanoparticles as the best content.

We investigated the angiogenesis-promoting properties of Cu₂O nanoparticles in vitro. We conducted cell migration and angiogenesis experiments and found that a concentration of 10

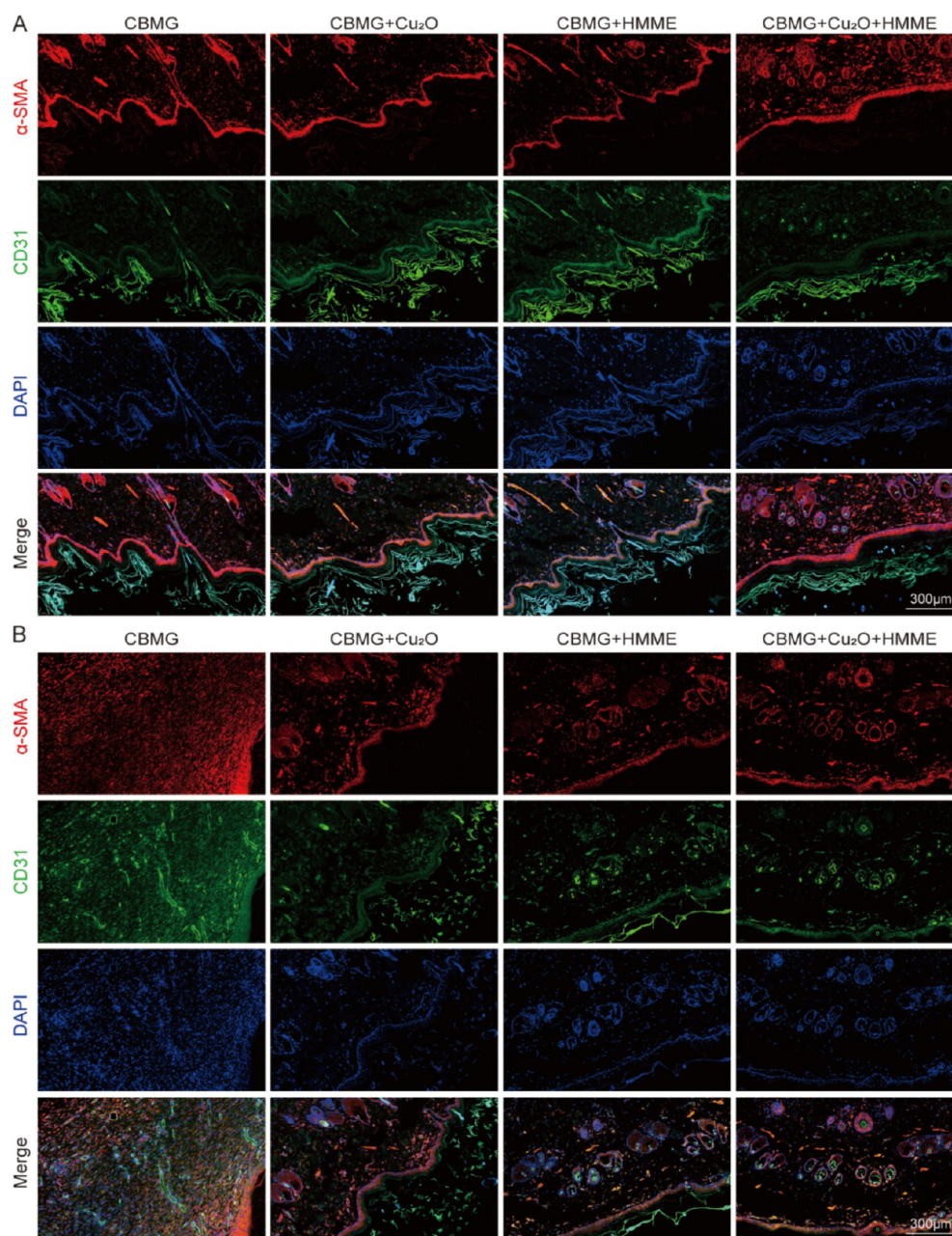


Figure 7. (A) Representative immunohistochemistry (IHC) images of CD31 and α -SMA with different hydrogels after 7 days ($n = 3$). (B) Representative immunohistochemistry images of CD31 and α -SMA treated with different hydrogels after 14 days ($n = 3$).

$\mu\text{g/mL}$ Cu₂O nanoparticles had the best effect on the cell migration and angiogenesis. These results were supported by quantitative analysis. It is well-known that revascularization is an imperative condition for skin defects, which would provide necessary materials such as oxygen and nutrients.²¹ In addition, the angiogenesis can participate in extracellular matrix forming.²² All of these advantages could accelerate the reconstruction of skin defects.²³ The Cu₂O nanoparticles could exert a positive influence on angiogenesis in some content. However, the concentration of Cu₂O needs to be redetermined, owing to the release difference with copper ions. According to the research referring to the content of Cu₂O, we determined the range of and concluded that 10 $\mu\text{g/mL}$ is the best choice in the CBMG hydrogel system.^{20,24}

The copper ions have some cytotoxicity in low concentrations; barely using copper ions to exert antibacterial

function or angiogenesis might lead to cytotoxicity effort. In addition, soluble copper ions in hydrogels would release more quickly than solid Cu₂O nanoparticles. If this side effect was alleviated by limiting the concentration of copper ions, the antibacterial efforts would be influenced regardless of lasting time or effective concentration. In this condition, Cu₂O nanoparticles are a good choice that would solve the question of cytotoxicity and efforts. It also needs to be known that the copper would disrupt the hydrogel-forming according to our preliminary experiment. It was attributed to the positive charges copper ions contained disturbing charge attraction among hydrogel ingredients. As for HMME, it is already applied in clinical treatments which indicates HMME is safe enough to for this career, and so does research.⁹ This work does not discuss the biocompatibility of HMME and takes it for granted that HMME is safe to use in this situation.

3.4. Antibacterial Performance of CBMG after Photo-Activated In Vitro. Antibacterial capacity is also an indispensable ability for hydrogels used for skin healing. MRSA and ESBL *Escherichia coli* were chosen as the model strains. In addition, the antibacterial ability of groups with HMME has been greatly improved after being treated with laser lighting, while simply using Cu₂O or HMME demonstrates an inferior antibacterial activity. Instead, the combination of them can effectively improve the antibacterial capacity (Figure 5A). Quantitative analysis confirms this view (Figure 5C). SEM further was employed to observe the bacterial morphology with different CBMG hydrogels under/underplus laser treatment. Results show that simple use of Cu₂O or HMME has a few effects on bacterial morphology, while the combination would break the bacteria (Figure 5B).

In this section, antibacterial capacity of CBMG hydrogels was evaluated. We used MRSA and ESBL *Escherichia coli* as model strains. The results showed that the combination of HMME and Cu₂O effectively improved the antibacterial capacity, while using Cu₂O or HMME alone demonstrated inferior antibacterial activity. SEM analysis further confirmed that the combination of HMME and Cu₂O had a significant effect on the bacterial morphology.

It is reported that a single use of Cu₂O could inhibit the bacterial activity.²⁵ In the previous step, the amount of Cu₂O nanoparticles was determined according to the demand of angiogenesis. Even if this condition is not the best choice for antibacterial usage, skin curing is the first aim we set for which we choose this concentration added to the CBMG hydrogel. The content of Cu₂O was determined in this concern. The results showed that Cu₂O is not the major ingredient in antibacterial applications. HMME has better efforts in killing bacteria than Cu₂O no matter whether laser lighting. The HMME can extremely improve the antibacterial ability especially when suffering laser treatment. In addition, HMME is also an ideal antibacterial drug,^{17,26} which was used in photodynamic therapy (PDT) and got positive results when treated with G⁺ bacterial,¹⁶ as well as G⁻ bacterial.²⁷

Even if HMME has better antibacterial efforts, the compound hydrogel system containing Cu₂O and HMME has the best results. The combination of these two participants in this research indicated that combination therapy could improve the effects. Numerous research studies support this opinion.²⁸ Our results reconfirm this strategy that the compound hydrogel has the potential in the clinical treatment of infected skin defects.

3.5. Skin Defect and Repair In Vivo. It is a wound dressing material that has promise for clinical transformation, and CBMG-Cu₂O-HMME was estimated in the skin infective defect model on Sprague–Dawley (SD) rats. To determine the wound healing rate, skin defect size was measured at setting time. Representing images are displayed in Figure 6A. According to quantitative analysis, the CBMG-Cu₂O-HMME group has the best healing after 3 days (Figure 6B). After 14 days, all groups were almost completely healed (Figure 6C). HE staining, Masson staining, and Sirius Red staining were used to estimate the skin healing. The results show that the defect gap shrinks (Figure 6D–F). Immunohistology is used to assess new blood vessels (Figure 7A,B). It shows that more new blood vessels in CBMG-Cu₂O-HMME demonstrate that the release of Cu²⁺ from hydrogel can contribute to angiogenesis.

To assess the potential of CBMG-Cu₂O-HMME as a wound dressing material, in vivo experiments were conducted on SD rats with skin infective defects. The researchers measured the wound healing rate and found that the CBMG-Cu₂O-HMME group had the best healing after 3 days, with all groups almost completely healing after 14 days. Histological staining and immunohistology were used to evaluate skin healing and the formation of new blood vessels. The results showed that the CBMG-Cu₂O-HMME group had a significant increase in the number of new blood vessels, indicating that the release of Cu²⁺ from the hydrogel contributed to angiogenesis.

4. CONCLUSIONS

In this research, a CBMG-Cu₂O-HMME hydrogel was developed by combining the carbomer hydrogel with Cu₂O and HMME through electrostatic interaction. The hydrogel exhibited enhanced photoactivated antibacterial activity compared to Cu₂O or HMME alone. The photophysical characterization confirmed the successful formation of the hydrogel, and biocompatibility tests demonstrated its safety and compatibility with human cells. In vitro experiments showed the angiogenesis-promoting ability of the hydrogel. Antibacterial performance was significantly improved when Cu₂O and HMME were combined with the hydrogel. In vivo experiments on a rat model confirmed the potential of the hydrogel for disinfection and repair of skin defects. Overall, the CBMG-Cu₂O-HMME hydrogel shows promise as a wound dressing material for infected wounds.

■ ASSOCIATED CONTENT

Data Availability Statement

Data sets in this article are confidential.

Supporting Information

The Supporting Information is available free of charge at <https://pubs.acs.org/doi/10.1021/acsomega.3c08718>.

Energy dispersive X-ray spectroscopy (EDS) analysis confirming the elemental composition of the CBMG hydrogel (PDF)

■ AUTHOR INFORMATION

Corresponding Authors

Ming Guan – Department of Orthopedic Surgery, The First Affiliated Hospital, College of Medicine, Zhejiang University, Hangzhou 310058, China; Department of Surgery, Beth Israel Deaconess Medical Center and Joslin-Beth Israel Deaconess Foot Center and the Rongxiang Xu, MD, Center for Regenerative Therapeutics, Beth Israel Deaconess Medical Center, Harvard Medical School, Boston, Massachusetts 02115, United States; Email: guanm@zju.edu.cn

Pengfei Lei – Department of Orthopedic Surgery, The First Affiliated Hospital, College of Medicine, Zhejiang University, Hangzhou 310058, China; Email: leipengfei@zju.edu.cn

Authors

Dongyu Wang – Department of Orthopedic Surgery, Xiangya Hospital Central South University, Changsha 410008, China; Department of Orthopedic Surgery, The First Affiliated Hospital, College of Medicine, Zhejiang University, Hangzhou 310058, China; orcid.org/0000-0002-4374-833X

Jiale Jin – Department of Orthopedic Surgery, The First Affiliated Hospital, College of Medicine, Zhejiang University, Hangzhou 310058, China

Chengran Zhang – Department of Orthopedic Surgery, Xiangya Hospital Central South University, Changsha 410008, China

Chengxin Ruan – Department of Orthopedic Surgery, The First Affiliated Hospital, College of Medicine, Zhejiang University, Hangzhou 310058, China

Yifang Qin – Department of Endocrinology, The Children's Hospital, School of Medicine, Zhejiang University, Zhejiang, Hangzhou 310052, China

Dongdong Li – Ningxia Medical University, Yinchuan, Ningxia 750004, China

Complete contact information is available at:

<https://pubs.acs.org/10.1021/acsomega.3c08718>

Author Contributions

Conceptualization was performed by D.W., J.J., and M.G. Data curation was done by J.J. and D.W. Formal analysis was done by D.W. Funding acquisition was performed by P.L. Investigation was done by D.W. and J.J. Methodology was developed by D.W. and C.R. Project administration was performed by D.W. Resources and software were procured by D.W. Supervision was done by M.G. Validation was performed by D.W. Visualization was done by C.Z., M.G., and D.W. Writing of the original draft was done by D.W., J.J., and M.G. Writing of the review and editing were performed by D.W., M.G., and J.J.

Funding

This study was supported by the Major science and technology projects of Changsha City (grant no. kh2003016). The Natural Science Foundation Exploration Project of Zhejiang Province, China (grant no. Y23H060040), the Natural Science Foundation of Hunan Province, China (grant no. 2022JJ30934), and the Medical and Health Research Project of Zhejiang province (2021KY153 and 2023KY098).

Notes

The authors declare no competing financial interest. All animal experiments received ethical approval by the Biomedical Research Ethics Committee of the First Affiliated Hospital, Zhejiang University. Not applicable.

ACKNOWLEDGMENTS

Not applicable.

REFERENCES

(1) Holmes, A. H.; Moore, L. S. P.; Sundsfjord, A.; Steinbakk, M.; Regmi, S.; Karkey, A.; Guerin, P. J.; Piddock, L. J. V. Understanding the mechanisms and drivers of antimicrobial resistance. *Lancet* **2016**, 387 (10014), 176–187. Willyard, C. The drug-resistant bacteria that pose the greatest health threats. *Nature* **2017**, 543 (7643), 15. From NLM.

(2) Zhao, Y.; Wang, Y.; Wang, X.; Qi, R.; Yuan, H. Recent Progress of Photothermal Therapy Based on Conjugated Nanomaterials in Combating Microbial Infections. *Nanomaterials* **2023**, 13 152269 DOI: 10.3390/nano13152269. From NLM. Han, J.; Zeng, S.; Chen, Y.; Li, H.; Yoon, J. Prospects of coupled iron-based nanostructures in preclinical antibacterial therapy. *Advanced drug delivery reviews* **2023**, 193, No. 114672. From NLM. Nguyen, V. N.; Zhao, Z.; Tang, B. Z.; Yoon, J. Organic photosensitizers for antimicrobial phototherapy. *Chem. Soc. Rev.* **2022**, 51 (9), 3324–3340. From NLM.

(3) Vinagreiro, C. S.; Zangirolami, A.; Schaberle, F. A.; Nunes, S. C. C.; Blanco, K. C.; Inada, N. M.; da Silva, G. J.; Pais, A. A. C. C.; Bagnato, V. S.; Arnaut, L. G.; et al. Antibacterial Photodynamic Inactivation of Antibiotic-Resistant Bacteria and Biofilms with Nanomolar Photosensitizer Concentrations. *ACS Infectious Diseases* **2020**, 6 (6), 1517–1526. Zhou, T.; Yin, Y.; Cai, W.; Wang, H.; Fan, L.; He, G.; Zhang, J.; Jiang, M.; Liu, J. A new antibacterial nano-system based on hematoporphyrin-carboxymethyl chitosan conjugate for enhanced photostability and photodynamic activity. *Carbohydr. Polym.* **2021**, 269, No. 118242. Hsia, T.; Small, J. L.; Yekula, A.; Batool, S. M.; Escobedo, A. K.; Ekanayake, E.; You, D. G.; Lee, H.; Carter, B. S.; Balaj, L. Systematic Review of Photodynamic Therapy in Gliomas. *Cancers* **2023**, 15 (15). DOI: 3918. From NLM.

(4) Wu, X.; Yang, M.; Kim, J. S.; Wang, R.; Kim, G.; Ha, J.; Kim, H.; Cho, Y.; Nam, K. T.; Yoon, J. Reactivity Differences Enable ROS for Selective Ablation of Bacteria. *Angewandte Chemie (International ed. in English)* **2022**, 61 (17), No. e202200808. From NLM.

(5) Mathur, A.; Parihar, A. S.; Modi, S.; Kalra, A. Photodynamic therapy for ESKAPE pathogens: An emerging approach to combat antimicrobial resistance (AMR). *Microbial pathogenesis* **2023**, 106307. DOI: 10.1016/j.micpath.2023.106307. From NLM. Shivalkar, S.; Arshad, F.; Sahoo, A. K.; Sk, M. P. Visible Light-Mediated Photoactivated Sulfur Quantum Dots as Heightened Antibacterial Agents. *ACS omega* **2022**, 7 (37), 33358–33364. From NLM.

(6) Tsolekile, N.; Nelana, S.; Oluwafemi, O. S. Porphyrin as Diagnostic and Therapeutic Agent. *Molecules* **2019**, 24 (14). DOI: 2669. From NLM.

(7) Zhao, X.; Luo, J.; Huang, Y.; Mu, L.; Chen, J.; Liang, Z.; Yin, Z.; Chu, D.; Han, Y.; Guo, B. Injectable Antiswelling and High-Strength Bioactive Hydrogels with a Wet Adhesion and Rapid Gelling Process to Promote Sutureless Wound Closure and Scar-free Repair of Infectious Wounds. *ACS Nano* **2023**, 17 (21), 22015–22034. From NLM.

(8) Hu, T.; Wang, Z.; Shen, W.; Liang, R.; Yan, D.; Wei, M. Recent advances in innovative strategies for enhanced cancer photodynamic therapy. *Theranostics* **2021**, 11 (7), 3278–3300. From NLM.

(9) Min, Z.; Jing, L.; Jun, Z.; Simeng, Q.; Zhaoyang, W.; Zhao, W.; Weihui, Z. Influential Factors in the Efficacy of Hemoporphin-Mediated Photodynamic Therapy for Port-wine Stains. *Lasers in medical science* **2023**, 38 1 162. . From NLM. Kang, J.; Liu, J. J.; Fang, Y. H.; Lin, Y. Y.; Gong, W.; Wang, H. Y.; Lin, L. H.; Xiao, X. M. Hemoporphin-Mediated Photodynamic Therapy for Port-Wine Stains on Extremities. *Dermatology and therapy* **2023**, 13 (8), 1857–1871. From NLM.

(10) Liu, X.; Yang, L.; Zhang, Q.; Yang, F.; Jiang, X. Four Cases of Port-Wine Birthmark Treated with Hematoporphyrin Monomethyl Ether-Mediated Photodynamic Therapy After Radioactive Nuclide Patch Therapy. *Clinical, cosmetic and investigational dermatology* **2023**, 16, 1667–1675. From NLM.

(11) Yang, S. Y.; Wu, K.; Zhang, Y.; Liu, H. X.; Li, P.; Wu, C.; Yan, K. L. 2D Ag Ion-Loaded Anionic Nanosheets for Polymer-Based Film with Durable Antibacterial Activities. *ACS omega* **2022**, 7 (38), 33858–33865. From NLM. Demirel, B.; Erol Taygun, M. Zinc Oxide-Doped Antibacterial Soda Lime Glass Produced as a Glass Container. *ACS omega* **2023**, 8 (10), 9257–9264. From NLM.

(12) Elabbasy, M. T.; Alshammari, M. H.; Zrieq, R.; El Bayomi, R. M.; Tahoun, A.; El-Morsy, M. A.; Abd El-Kader, M. F. H. Physical and biological changes of copper oxide and hydroxyapatite filled in polycaprolactone scaffolds: Cellular growth behavior and antibacterial activity. *Journal of the mechanical behavior of biomedical materials* **2023**, 144, No. 105927. From NLM. Li, H.; Zhang, L.; Zhang, X.; Zhu, G.; Zheng, D.; Luo, S.; Wu, M.; Li, W. H.; Liu, F. Q. Self-Enhanced Antibacterial and Antifouling Behavior of Three-Dimensional Porous Cu(2)O Nanoparticles Functionalized by an Organic-Inorganic Hybrid Matrix. *ACS Appl. Mater. Interfaces* **2023**, 15 (32), 38808–38820. From NLM. Qiao, Y.; He, J.; Chen, W.; Yu, Y.; Li, W.; Du, Z.; Xie, T.; Ye, Y.; Hua, S. Y.; Zhong, D.; et al. Light-Activatable Synergistic Therapy of Drug-Resistant Bacteria-Infected Cutaneous Chronic Wounds and Nonhealing Keratitis by Cupriferous Hollow Nanoshells. *ACS Nano* **2020**, 14 (3), 3299–3315. From NLM.

- (13) Wang, Z.; Xue, Y.; Zhu, Z.; Hu, Y.; Zeng, Q.; Wu, Y.; Wang, Y.; Shen, C.; Jiang, C.; Liu, L. et al. Quantitative Structure-Activity Relationship of Enhancers of Licochalcone A and Glabridin Release and Permeation Enhancement from Carbomer Hydrogel. *Pharmaceutics* **2022**, *14*, 2262 DOI: 10.3390/pharmaceutics14020262. From NLM. Chen, J.; Wang, Z.; Sun, J.; Zhou, R.; Guo, L.; Zhang, H.; Liu, D.; Rong, M.; Ostrikov, K. K. Plasma-Activated Hydrogels for Microbial Disinfection. *Adv. Sci.* **2023**, *10* (14), No. e2207407. From NLM. Hu, Y.; Liang, P.; Wang, Z.; Jiang, C.; Zeng, Q.; Shen, C.; Wu, Y.; Liu, L.; Yi, Y.; Zhu, H.; et al. Exploring the mechanism of solubilization and release of isoliquiritigenin in deep eutectic solvents. *International journal of pharmaceutics* **2023**, *644*, No. 123298. From NLM.
- (14) Liang, M.; Shang, L.; Yu, Y.; Jiang, Y.; Bai, Q.; Ma, J.; Yang, D.; Sui, N.; Zhu, Z. Ultrasound activatable microneedles for bilaterally augmented sono-chemodynamic and sonothermal antibacterial therapy. *Acta Biomaterialia* **2023**, *158*, 811–826. Wang, X.; Li, Q.; Miao, Y.; Chen, X.; Zhang, X.; Shi, J.; Liu, F.; Wang, X.; Li, Z.; Yang, Y.; et al. A 0D-2D Heterojunction Bismuth Molybdate-Anchored Multifunctional Hydrogel for Highly Efficient Eradication of Drug-Resistant Bacteria. *ACS Nano* **2023**, *17* (16), 15568–15589.
- (15) Guan, M.; Chu, G.; Jin, J.; Liu, C.; Cheng, L.; Guo, Y.; Deng, Z.; Wang, Y. A Combined Cyanine/Carbomer Gel Enhanced Photodynamic Antimicrobial Activity and Wound Healing. *Nanomaterials* **2022**, *12* (13), 2173 DOI: 10.3390/nano12132173. From NLM.
- (16) Ma, W.; Wang, T. Study of hematoporphyrin monomethyl ether-mediated blue-light photodynamic therapy in the treatment of oral ulcers infected with *Staphylococcus aureus*: In vivo evaluation. *Photodiagnosis and photodynamic therapy* **2023**, *42*, No. 103363. From NLM.
- (17) Liu, C.; Hu, M.; Ma, D.; Lei, J.; Xu, J. Photodynamic inactivation of antibiotic-resistant bacteria and biofilms by hematoporphyrin monomethyl ether. *Lasers in medical science* **2016**, *31* (2), 297–304. From NLM.
- (18) Song, H.; Wang, W.; Zhao, P.; Qi, Z.; Zhao, S. Cuprous oxide nanoparticles inhibit angiogenesis via down regulation of VEGFR2 expression. *Nanoscale* **2014**, *6* (6), 3206–3216. From NLM.
- (19) Saghiri, M. A.; Asatourian, A.; Orangi, J.; Sorenson, C. M.; Sheibani, N. Functional role of inorganic trace elements in angiogenesis-Part II: Cr, Si, Zn, Cu, and S. *Critical reviews in oncology/hematology* **2015**, *96* (1), 143–155. From NLM. Amer, T. A. M.; Palanisamy, S.; So, P. B.; Vijayaraghavan, P.; Tzou, S. C.; Lu, T. T.; Lin, C. H.; Wang, Y. M. Sustained Releasable Copper and Zinc Biogenic Ions Co-Assembled in Metal-Organic Frameworks Reinforced Bacterial Eradication and Wound Mitigation in Diabetic Mice. *Bioconjugate Chem.* **2023**, *34*, 1688. From NLM.
- (20) Chen, J.; He, J.; Yang, Y.; Qiao, L.; Hu, J.; Zhang, J.; Guo, B. Antibacterial adhesive self-healing hydrogels to promote diabetic wound healing. *Acta Biomater* **2022**, *146*, 119–130. From NLM.
- (21) Frueh, F. S.; Sanchez-Macedo, N.; Calcagni, M.; Giovanoli, P.; Lindenblatt, N. The Crucial Role of Vascularization and Lymphangiogenesis in Skin Reconstruction. *European surgical research. Europäische chirurgische Forschung. Recherches chirurgicales europeennes* **2018**, *59* (3–4), 242–254. From NLM.
- (22) Bi, H.; Li, H.; Zhang, C.; Mao, Y.; Nie, F.; Xing, Y.; Sha, W.; Wang, X.; Irwin, D. M.; Tan, H. Stromal vascular fraction promotes migration of fibroblasts and angiogenesis through regulation of extracellular matrix in the skin wound healing process. *Stem cell research & therapy* **2019**, *10* (1), 302. From NLM.
- (23) Li, Y.; Jiang, Q. L.; Van der Merwe, L.; Lou, D. H.; Lin, C. Preclinical efficacy of stem cell therapy for skin flap: a systematic review and meta-analysis. *Stem cell research & therapy* **2021**, *12* (1), 28. From NLM. Li, Y.; Duan, W.; Shen, L.; Ma, X.; Ma, J.; Zhang, Y.; Guo, Y. Shengji solution accelerates the wound angiogenesis of full-thickness skin defect in rats via activation of TGF- β 1/Smad3-VEGF signaling pathway. *Biotechnol. Genetic Eng. Rev.* **2023**, 1–18. From NLM. Im, H.; Kim, S. H.; Kim, S. H.; Jung, Y. Skin Regeneration with a Scaffold of Predefined Shape and Bioactive Peptide Hydrogels. *Tissue engineering. Part A* **2018**, *24* (19–20), 1518–1530. From NLM.
- (24) Li, S.; Zhang, L.; Liu, C.; Kim, J.; Su, K.; Chen, T.; Zhao, L.; Lu, X.; Zhang, H.; Cui, Y.; Cui, X.; Yuan, F.; Pan, H.; et al. Spontaneous immunomodulation and regulation of angiogenesis and osteogenesis by Sr/Cu-borosilicate glass (BSG) bone cement to repair critical bone defects. *Bioact. Mater.* **2023**, *23*, 101–117. From NLM.
- (25) Athinarayanan, J.; Periasamy, V. S.; Krishnamoorthy, R.; Alshatwi, A. A. Evaluation of antibacterial and cytotoxic properties of green synthesized Cu(2)O/Graphene nanosheets. *Materials science & engineering. C, Materials for biological applications* **2018**, *93*, 242–253. From NLM.
- (26) Zhang, Y.; Zhang, H.; Zhuang, D.; Bi, L.; Hu, Z.; Cao, W. Hematoporphyrin monomethyl ether mediated sonodynamic antimicrobial chemotherapy on *porphyromonas gingivalis* in vitro. *Microbial pathogenesis* **2020**, *144*, No. 104192. From NLM.
- (27) Zhang, M.; Cui, Z.; Wang, Y.; Ma, W.; Ji, Y.; Ye, F.; Feng, Y.; Liu, C. Effects of sub-lethal antimicrobial photodynamic therapy mediated by hematoporphyrin monomethyl ether on polymyxin-resistant *Escherichia coli* clinical isolate. *Photodiagnosis and photodynamic therapy* **2021**, *36*, No. 102516. From NLM.
- (28) Fu, X.; Ni, Y.; Wang, G.; Nie, R.; Wang, Y.; Yao, R.; Yan, D.; Guo, M.; Li, N. Synergistic and Long-Lasting Wound Dressings Promote Multidrug-Resistant *Staphylococcus Aureus*-Infected Wound Healing. *Int. J. Nanomedicine* **2023**, *18*, 4663–4679. From NLM. Luo, H.; Yin, X. Q.; Tan, P. F.; Gu, Z. P.; Liu, Z. M.; Tan, L. Polymeric antibacterial materials: design, platforms and applications. *Journal of materials chemistry. B* **2021**, *9* (12), 2802–2815. From NLM. Aydin, A.; Ulag, S.; Sahin, A.; Aksu, B.; Gunduz, O.; Ustundag, C. B.; Marinas, I. C.; Georgescu, M.; Chifiriuc, M. C. Biocompatible polyvinyl alcohol nanofibers loaded with amoxicillin and salicylic acid to prevent wound infections. *Biomedical materials* (Bristol, England), **2023**. DOI: DOI: 10.1088/1748-605X/acf25c. From NLM.